Coupled urban-topographic interactions in a complex mountainous valley: A WRF-based evaluation of urban morphology effects on pre-monsoon temperature regimes in the Doon Valley, India

Ujjwal Kumar, Deepak Kumar

School of Environment & Natural Resources, Doon University, Dehradun, India

Vikas Singh

National Atmospheric Research Laboratory (NARL), ISRO, Tirupati, India

Abstract

In this study, we investigate the influence of urban morphology on pre-monsoon temperature regimes in the Doon Valley, a complex intermontane basin in the western Himalayas, using high-resolution (2×2 km²) Weather Research and Forecasting (WRF) model simulations for the year 2021. The model employed a threefold nested domain (18-6-2 km) configuration with National Centers for Environmental Prediction – Final Analysis (NCEP-FNL) (0.25°×0.25°) global analyses as boundary conditions. To represent the rapidly expanding built environment of Dehradun, a simulation incorporating the Urban Canopy Model with the Building Effect Parameterization (WRF-UCM-BEP) was conducted and validated against ground-based observations from both Dehradun (urbanized valley, ~640 m ASL) and Mussoorie (hill station, ~2005 m ASL). The inclusion of urban canopy physics markedly improved model performance in Dehradun, reducing mean absolute error and root mean square error by 15-20% relative to the control run and increasing correlation and agreement for ambient (2 m) air temperature ($r = 0.83 \rightarrow 0.86$; index of agreement = 0.72 → 0.78). In contrast, improvements in Mussoorie were marginal, confirming that urbanization-driven heat storage and morphology dominate thermal behavior within the valley city. The WRF-UCM-BEP simulation effectively reproduced the ambient urban heat island (UHI), with persistent nighttime warming of 1-2°C over Dehradun's city core and a more realistic diurnal cycle. The model also improved representation of the surface UHI, showing stronger spatial coherence and closer agreement with MODIS 1 km land-surface temperature patterns. Vertical diagnostics revealed that WRF-UCM-BEP improved the vertical depiction of boundary-layer structure, weakening katabatic winds (−1.5 to −2 m s^{-1}), suppressing nocturnal inversion, and capturing elevated warm layers consistent with observed mixing profiles. The results demonstrate that urban morphology exerts dominant control over both ambient and surface thermal environments in Dehradun, underscoring the importance of realistic multilayer urban-canopy parameterizations in high-resolution, nested mesoscale modeling of Himalayan cities.

Keywords

WRF model, Urban Canopy Model, Building Effect Parameterization, mountain breeze circulation, Himalayan Terrain, Urban Heat Island, High-Resolution Simulation.

Submitted 12 July 2025, revised 29 October 2025, accepted 15 December 2025

DOI: 10.26491/mhwm/215597

1. Introduction

Numerical weather prediction (NWP) models such as the Weather Research and Forecasting (WRF) model (Skamarock et al. 2019) have become indispensable tools for simulating atmospheric processes, and have been extensively used over complex mountainous terrains (Zhang et al. 2013; Karki et al. 2017; Arthur et al. 2018; Luna et al. 2020; Navale, Singh 2020; Golzio et al. 2021; Min et al. 2021; Singh et al. 2021; Zhang et al. 2022; Liu et al. 2023; Biswasharma et al. 2024). However, the performance of these models is sensitive to topography, grid size, and the choice of physical parameterization schemes,

including planetary boundary layer (PBL) schemes, microphysics, and cumulus parameterizations (Arthur et al. 2018; Navale, Singh 2020; Singh et al. 2021; Golzio et al. 2021; Liu et al. 2024; Singh et al. 2024b).

Previous studies have demonstrated the importance of high-resolution WRF simulations in improving meteorological representation in mountainous regions. For example, Zhang et al. (2013) applied a probability matching approach to correct satellite rainfall biases using WRF simulations, while Karki et al. (2017) evaluated WRF performance at multiple resolutions (25, 5, and 1 km) over the Khumbu and Rolwaling regions, highlighting that finer resolutions capture monsoonal precipitation peaks more realistically. Arthur et al. (2018) introduced topographic shading and slope effects in WRF through the Immersed Boundary Method, showing improvements in surface energy fluxes and thermally driven flows. Similarly, Luna et al. (2020) improved meteorological simulations over Bogotá by replacing the default elevation with Alos-PALSAR DEM data. These examples demonstrate that WRF's ability to represent local climate strongly depends on topographic representation and resolution.

Topographic modifications also alter atmospheric instability. For instance, Navale and Singh (2020) used WRF experiments over the Northwest Himalayas, finding that variables such as relative humidity, convective available potential energy (CAPE), and wind speed respond significantly to changes in elevation and valley representation. Golzio et al. (2021) emphasized the influence of land-use datasets on simulations over the Italian Alps, while Singh et al. (2021) showed that finer resolution reduces biases in Central Himalayan simulations compared to Ganges Valley Aerosol Experiment (GVAX) observations. More recently, Liu et al. (2023, 2024) highlighted the sensitivity of WRF precipitation to microphysics, cumulus, and Planetary Boundary Layer (PBL) schemes over the Tibetan Plateau. Collectively, these studies stress that WRF simulations over complex terrain demand careful design of physics options and boundary conditions.

Urban morphology adds another layer of complexity. The incorporation of UCM and BEP into WRF has enabled researchers to capture urban heat island (UHI) effects and altered boundary-layer processes. For example, Lin et al. (2016) demonstrated improvements in diurnal air temperature simulation over Taiwan with UCM modifications, while Gaur et al. (2021) and Silva et al. (2021) showed that multilayer urban schemes better represent wind, humidity, and temperature extremes in Ottawa and Lisbon, respectively. Bilang et al. (2022) applied WRF-UCM to Manila and found improved simulation of high-heat events, and Roukounakis et al. (2023) highlighted the statistical significance of UCM inclusion over Athens. These findings confirm that representing urban morphology is essential for simulating near-surface meteorology in cities.

Despite these advances, studies coupling WRF-UCM over complex mountainous valleys that host rapidly urbanizing cities remain scarce. Intermontane basins such as the Doon Valley in Uttarakhand, India, present a unique challenge where urban expansion interacts with steep topography and thermally driven circulation. These considerations motivate the present study, which aims to evaluate high-resolution WRF simulations (2×2 km²) over the Doon Valley, compare them with ERA5, validate them against ground-

based observations, and explicitly assess the role of urban morphology through the UCM-BEP scheme. Specifically, we test whether including urban morphology improves simulation of temperature regimes during the pre-monsoon season, when urban heat effects are climatologically strongest.

2. Methodology

2.1. Study area

The Doon Valley, in the western Himalayan region of India within the state of Uttarakhand, forms an elongated intermontane depression bordered by the Siwalik Hills to the south and the Mussoorie Range (Lesser Himalaya**)** to the north. The domain spans 29.8°N – 31.2°N and 77.2°E – 78.8°E (Fig. 1). The valley's physiographic configuration results from the tectonic interplay between the Main Boundary Thrust (MBT) and the Himalayan Frontal Fault (HFF), which created a broad synclinal basin filled with Quaternary alluvium and piedmont deposits (Valdiya 1980; Thakur, Rawat 1992). Elevation ranges from about 400 m in the southern plains to over 2000 m along the northern ridges, establishing a steep north-south gradient that strongly influences thermal stratification and wind systems.

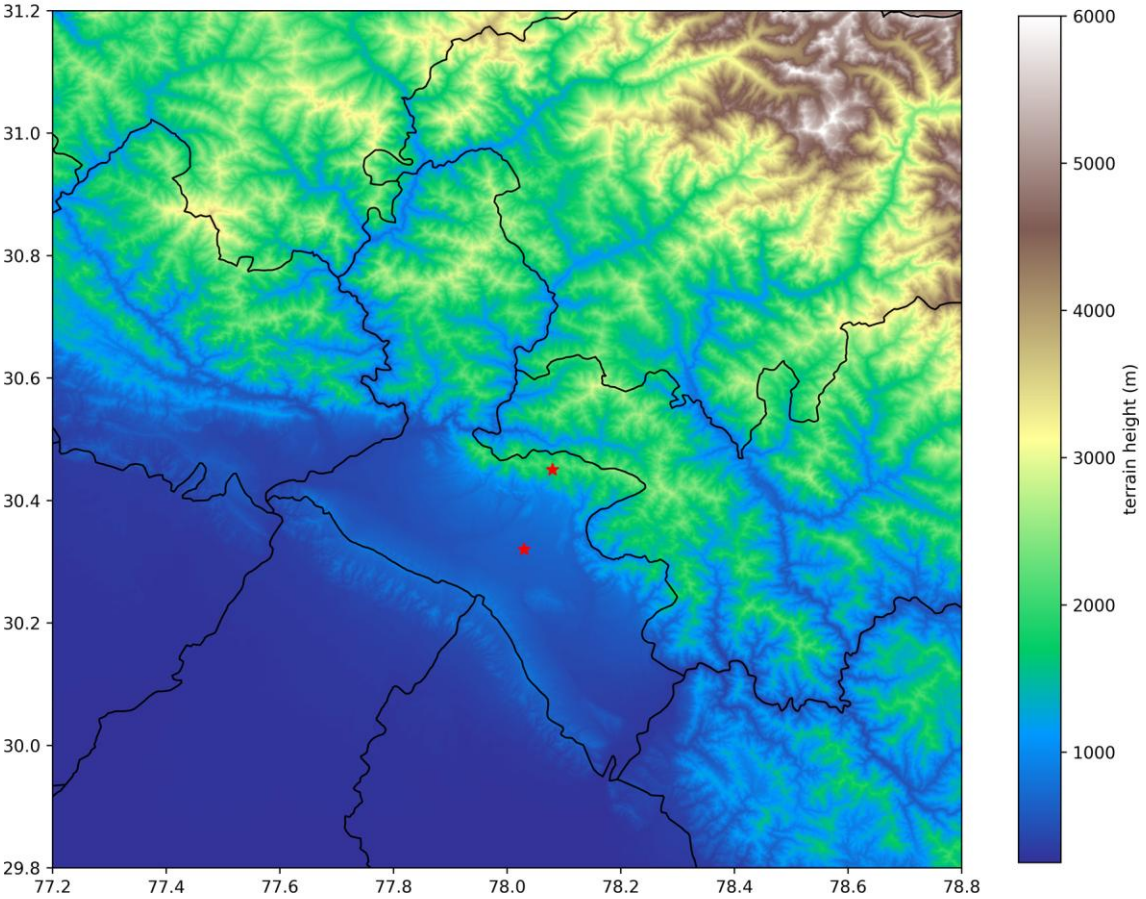

Fig. 1. Terrain of the study domain. The central area is the Dehradun district (Doon Valley area). The two red stars are the locations of IMD observation stations: Dehradun Mokhampur (30.32°N, 78.03°E, ~640 m altitude) and Mussoorie (30.45°N, 78.08°N, ~2005 m altitude). The map was prepared from the data of SRTM V3 product (SRTM Plus) provided by NASA JPL at a resolution of 1 arc-second (Farr et al. 2007).

This complex topography fosters diurnally reversing thermally driven circulations, characterized by daytime upslope (anabatic) and nighttime downslope (katabatic) winds, which play a crucial role in regulating the valley's temperature and ventilation (Karki et al. 2017). At the basin floor lies Dehradun, the capital of Uttarakhand (~640 m ASL), which has undergone rapid urban expansion in recent decades. The juxtaposition of this highly urbanized valley city with the adjacent Mussoorie hill station (~2005 m ASL) – a relatively undisturbed, forest-dominated region – creates a natural laboratory for studying urban-topographic interactions and the modulation of temperature regimes and urban heat island (UHI) effects in a mountainous environment.

Figure 1 shows the terrain configuration of the study domain derived from the SRTM V3 (1-arc-second) digital elevation model (DEM) provided by NASA JPL (Farr et al. 2007). The Dehradun district (central area) represents the core of the Doon Valley; the two red stars indicate the locations of the India Meteorological Department (IMD) stations at Dehradun Mokhampur (30.32°N, 78.03°E, ~640 m) and Mussoorie (30.45°N, 78.08°E, ~2005 m). The steep elevation contrast between these stations highlights the valley's orographic control on local meteorology.

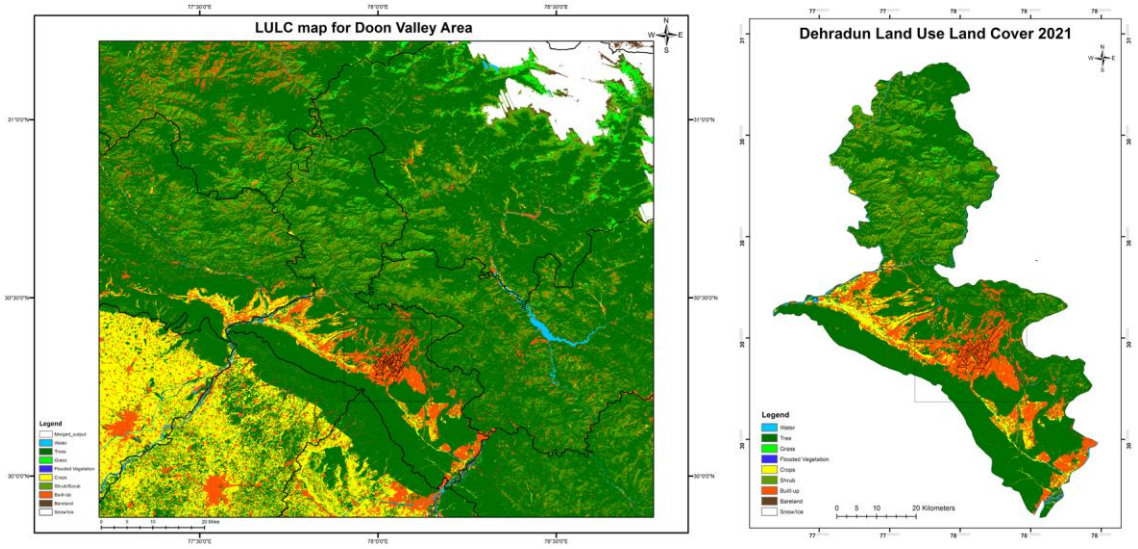

Fig. 2. Land use/land cover (LULC) for: the Doon Valley area (left map); the Dehradun district. The region shaded in red shows the built-up area (urban region) (right map). The region inside the dotted rectangular boundary in both (a) and (b) is the Dehradun city municipal area. The LULC map was obtained using a dynamic world dataset, which is a 10 m near-real-time (NRT) LULC dataset derived from Sentinel-2 L1C collection (Brown et al. 2022). The region shown within the dotted line in (a) shows Dehradun city and its surroundings.

Figure 2 presents the LULC distribution derived from the Dynamic World 10 m near-real-time dataset (Brown et al. 2022). Built-up areas (shown in red) are concentrated around the Dehradun municipal region, delineated by the dotted rectangular boundary, whereas surrounding areas are predominantly agricultural or forested. This spatial heterogeneity emphasizes the interplay between urban surfaces and natural terrain, which governs energy exchange, boundary-layer structure, and diurnal thermal gradients.

Thus, the Doon Valley offers a natural laboratory to study coupled urban-topographic interactions under pre-monsoon conditions, where both steep terrain and rapid urbanization jointly shape temperature distribution, local circulations, and the evolution of UHI phenomena.

2.2. WRF model

The Advanced Research WRF (ARW) modeling system version 4.2 (Skamarock et al. 2019) was used to simulate meteorology over the Doon Valley from 22 December 2020 to 1 January 2022, covering the full calendar year 2021. The first 10 days (22-31 December 2020) were treated as the model spin-up period. The year 2021 was selected because: (1) it represents a recent year with complete availability of high-quality IMD station data at both valley (Dehradun) and hill (Mussoorie) sites, and (2) it exhibited typical pre-monsoon conditions (March-June) with multiple heat events, making it suitable for UHI evaluation.

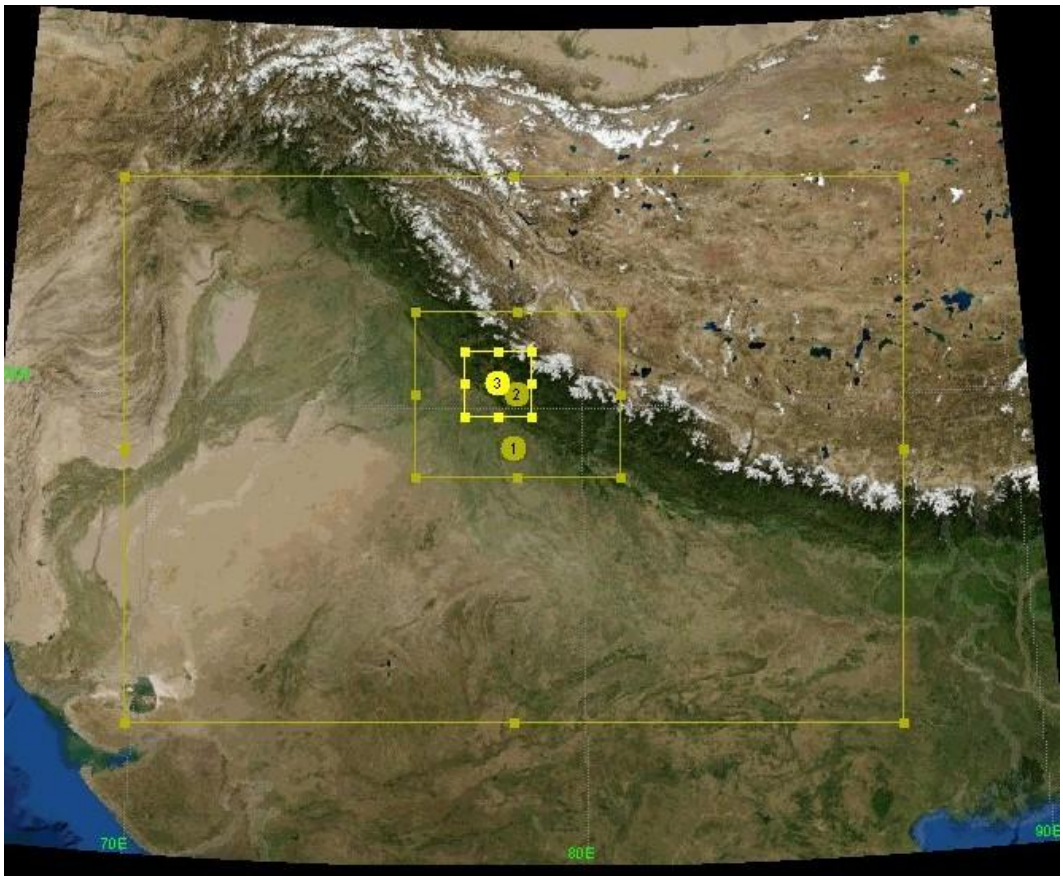

Fig. 3. The three-fold (1:3 ratio) nested domain (D01: 18×18 km^2, D02: 6×6 km^2, D03: 2×2 km^2) for WRF model set-up in the present study [obtained through WRF-domain wizard (NCAR 2008)]. The yellow circles 1, 2, and 3 depict the centers of domains D01, D02, and D03.

The WRF model employs a fully compressible, non-hydrostatic dynamical core with terrain-following vertical coordinates. Three nested domains (1:3 ratio) were used at 18 km, 6 km, and 2 km resolution, respectively, with the innermost domain focused on the Doon Valley (Fig. 3). Boundary conditions were derived from NCEP GDAS/FNL 0.25° global analyses. The following physical parameterizations were applied, based on prior Himalayan studies (Navale, Singh 2020; Singh et al. 2021; 2024b):

- Microphysics: WSM 3-class scheme (Hong et al. 2004).
- Planetary Boundary Layer (PBL): YSU scheme (Hong et al. 2006).
- Cumulus physics: Kain-Fritsch scheme (Kain 2004).
- Surface layer: Monin-Obukhov scheme (Monin, Obukhov 1954; Namdev et al. 2024).
- Land surface: Noah LSM (Ek et al. 2003).
- Longwave radiation: RRTM (Mlawer et al. 1997).

2.3. Urban Canopy Model – Building Effect Parameterization (UCM-BEP)

To represent urban canopy, we used the multilayer Building Effect Parameterization (BEP) scheme (Martilli et al. 2002; Mussetti et al. 2020; Hendricks, Knievel 2022), an option in WRF v4.2. The Urban Canopy Model BEP simulation was run for the pre-monsoon period (21 March – 30 June 2021, considering 21-Mar to 31-Mar as the spin-up period), during summer when UHI effects are strongest.

Unlike the single-layer UCM, BEP discretizes the urban canopy into multiple vertical layers and explicitly treats heat and momentum exchanges between roofs, walls, and roads. The momentum equation in BEP is:

$$\frac{\partial u}{\partial t} = -\frac{1}{\rho}\frac{\partial p}{\partial x} + \nu\frac{\partial^2 u}{\partial z^2} - C_D.\frac{A(z)}{V(z)}.u|u| \quad (1)$$

where:

- u is the horizontal wind component,
- C_D is the drag coefficient for buildings,
- $\frac{A(z)}{V(z)}$ is the ratio of building frontal area to volume at height z,
- ν is the eddy viscosity.

The energy balance in each urban layer is calculated for three distinct surfaces: roof**,** wall, and road. Each surface has its own surface energy balance:

$$Q^* = Q_H + Q_E + Q_C + Q_A \quad (2)$$

where:

- Q^* is the net radiation,
- Q_H is the sensible heat flux,
- Q_E is the latent heat flux,
- Q_G is the ground (or conductive) heat flux,
- Q_A is the anthropogenic heat flux (redundant in this study).

The vertical profiles of temperature, humidity, and wind are updated using these energy and momentum exchanges at each model level within the urban canopy, thereby improving the representation of the urban boundary layer (UBL) structure (Mussetti et al. 2020).

In this study, the NOAH land surface model (LSM) (Ek et al. 2003) was used in conjunction with the BEP-UCM framework to provide realistic treatment of soil moisture, evapotranspiration, and urban land-use interactions. The NOAH LSM supports the coupling of BEP with surface processes by enabling separate treatment of vegetated and impervious surfaces. The urban classification in the land-use data set (based on MODIS/USGS) triggers the UCM-BEP parameterizations over urban grid cells. Further, the BEP module enables building morphology parameters (e.g., average building height, street width, building fraction) to be user-specified or retrieved from lookup tables, facilitating more accurate representation of urban heterogeneity in grid-scale simulations. The default values used for Dehradun city were: average building height = 7.5 m, building width = 15 m, street width = 20 m, and impervious fraction = 0.9, typical of high-density urban cores (Garuma 2018). By explicitly resolving radiative trapping and dynamic drag in street canyons, the WRF-UCM-BEP system captures the thermal inertia of urban areas, their delayed nighttime cooling, and their suppression of thermally driven flows, which are critical to simulating urban heat island (UHI) effects in mountainous regions like the Doon Valley.

2.4. ERA-5 data

The ERA5 global reanalysis from the European Centre for Medium-Range Weather Forecasts (ECMWF) was used to evaluate large-scale temperature patterns. ERA5 employs the Integrated Forecasting System (IFS) Cycle 41r2 with a four-dimensional variational (4D-Var) data assimilation scheme that incorporates satellite, radiosonde, aircraft, and land observations. It provides hourly data at 0.25° (~31 km) resolution on 137 model levels. For improved near-surface representation, we used the ERA5-Land subset at 0.1°×0.1° (~9 km) resolution, which re-runs the IFS land component (HTESSEL) with enhanced land-surface and boundary-layer physics (Copernicus Climate Data Store 2024). ERA5-Land provides hourly temperature, soil, and flux variables with better land heterogeneity and topographic detail. In this study, ERA5-Land data for January-December 2021 were retrieved from the Copernicus Climate Data Store (CDS) and bilinearly interpolated to the WRF outer domain for consistent comparison with model outputs over the Doon Valley.

2.5. Surface observation data

Hourly meteorological observations were obtained from India Meteorological Department (IMD) stations at Dehradun Mokhampur (30.32°N, 78.03°E, 640 m) and Mussoorie (30.45°N, 78.08°E, 2005 m) (locations shown in Fig. 1). These served as the reference for validating WRF outputs.

2.6. Evaluation metrics

To evaluate the WRF simulation against the ground-based observations, we used the statistical metrics correlation (r), root mean square error ($RMSE$), index of agreement (IOA), mean absolute error (MAE), mean absolute percentage error ($MAPE$), and normalized root mean square error $(NRMSE)$ (Willmott 1981; Karppinen et al. 2000; Borrego et al. 2008).

$$CORR = \frac{\sum_{i=1}^{n}(S_i-\bar{S})(O_i-\bar{O})}{\sqrt{\sum_{i=1}^{n}(S_i-\bar{S})^2}\sqrt{\sum_{i=1}^{n}(O_i-\bar{O})^2}} \quad (3)$$

$$IOA = 1 - \frac{\sum_{i=1}^{n}(S_i-O_i)^2}{\sum_{i=1}^{n}(|S_i-\bar{O}|+|O_i-\bar{O}|)^2} \quad (4)$$

$$RMSE = \sqrt{\frac{1}{n}\sum_{i=1}^{n}(S_i - O_i)^2} \quad (5)$$

$$MAE = \frac{1}{n}\sum_{i=1}^{n}|S_i - O_i| \quad (6)$$

$$MAPE = \frac{100}{n}\sum_{i=1}^{n}\left|\frac{S_i-O_i}{O_i}\right| \quad (7)$$

$$NRMSE = \frac{RMSE}{\bar{O}} \times 100 \quad (8)$$

where S_i and O_i are simulated and observed values, n is the number of samples, and $\bar{O}$ and $\bar{S}$ are the means of observed and simulated values.

3. Results and discussion

The WRF simulation was run for the entire year 2021, spanning from 22 Dec 2020 to 01 Jan 2022, with a model spin-up period of 22-31 Dec 2020. The simulation covered the domain 29.8°N to 31.2°N and 77.2°E to 78.8°E, the Doon Valley region, at 2×2 km² resolution. The WRF simulation was carried out in three nested domains (18×18 km², 6×6 km², 2×2 km²). As discussed in the Methods section, the WRF physics schemes were chosen in view of earlier WRF studies of the same region that provided optimum results, i.e., the YSU scheme for the boundary layer (Navale, Singh 2020; Singh et al. 2024b). The high-resolution WRF meteorological simulations have been compared with 0.1°×0.1° resolution ERA-5 to assess the effect of high-resolution distinctive features. The WRF simulated meteorology has been evaluated against ground-based observations for an entire year at the valley site (Dehradun) and the hill site (Mussoorie). Dehradun has become highly urbanized in recent decades; hence, WRF with the Urban Canopy Model (UCM) using the BEP scheme has been run over the region, and the performance of WRF and WRF-UCM has been compared.

3.1. High resolution features: WRF simulation at 2 x 2 km resolution vs. ERA-5 Land data at 0.1°×0.1° resolution

The WRF meteorological simulation for 2 m temperature and 2 m relative humidity, and its comparison with ERA-5 Land data at 0.1°×0.1° resolution, are presented in Figures 4 and 5. The WRF simulated at higher resolution, allowing it to capture small-scale temperature variations in greater detail. This feature is evident in the more granular patterns (Jun-2021), especially in the valley and hilly regions. The ERA-5 Land data (right) has a coarser resolution (~10 km), leading to a smoother representation of temperature variations over the region; however, the finer details, such as local temperature variations in valleys and ridges, are not well captured. The WRF model is better at capturing local heating and cooling effects, likely

influenced by elevation, land use, and terrain. This enhancement is important for valleys like Doon, where complex topography plays a significant role in temperature distribution. The ERA-5 data set, while useful for large-scale trends, cannot resolve fine-scale topographic influences as effectively as WRF's higher resolution simulation. The wintertime (January 2021) comparison shows that WRF exhibits stronger cooling in the north (blue shading), corresponding to hill and mountainous areas, while southern valley regions remain warmer, showing the expected winter temperature inversion. Colder regions are less pronounced in ERA-5, suggesting weaker resolution of temperature inversion effects in the valley.

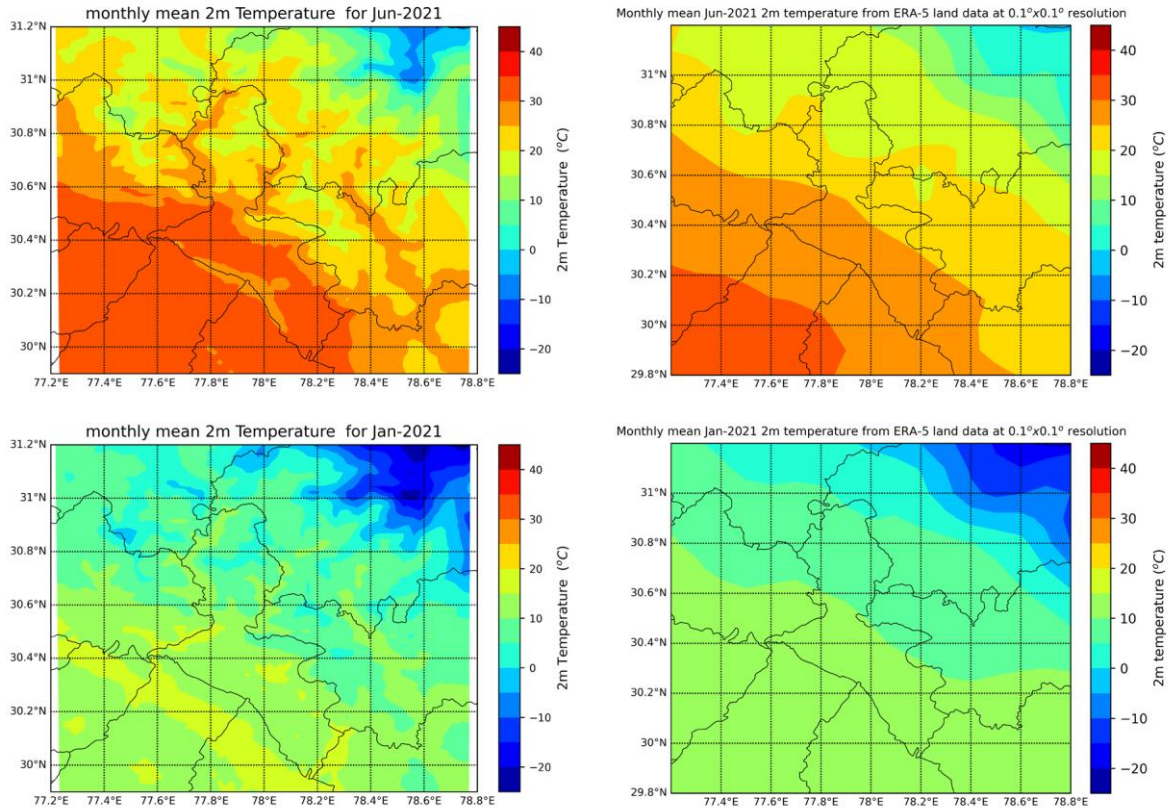

Fig. 4. Comparison of 2 m temperature from WRF (2×2 km² resolution) simulation (left) and ERA-5 (0.1°×0.1°) resolution (right) for June 2021 (upper panels) and January 2021 (lower panels).

Figure 5 compares 2 m relative humidity (RH) between the WRF (2×2 km²) simulation and ERA-5 (0.1°×0.1°) data for the monsoon season (July 2021) and the pre-monsoon season (April 2021). In the monsoon season (July 2021), WRF captures significant spatial variability in RH, especially over hilly areas where RH is locally higher. It shows pockets of high RH (>80%) in northern and central regions, likely the effect of orographic lifting causing moisture accumulation. Sharp humidity gradients are evident, reflecting terrain influence on moisture distribution. The ERA-5 results show a smoother distribution of RH with a large-scale gradient from south (~40-50%) to north (~80%). It lacks the fine-scale humidity variations caused by local terrain effects. The WRF's high resolution simulation captures orographic moisture enhancement due to monsoon winds interacting with the terrain. As seen in WRF, orographic lifting causes higher RH over hills, an effect not well-represented in ERA-5. Evidently, the local

convective systems, which increase humidity locally, are better captured in WRF. In the pre-monsoon season (April 2021), the WRF shows widespread lower RH (<40%), especially in the southern and central parts of the region, while there is higher RH in some northern areas, likely due to local moisture retention in higher-altitude regions.

The ERA-5 depicts a more uniform humidity field, lacking the local variations seen in WRF, showing higher RH (~50-60%) over northern areas, but the distribution of lower RH is smoother.

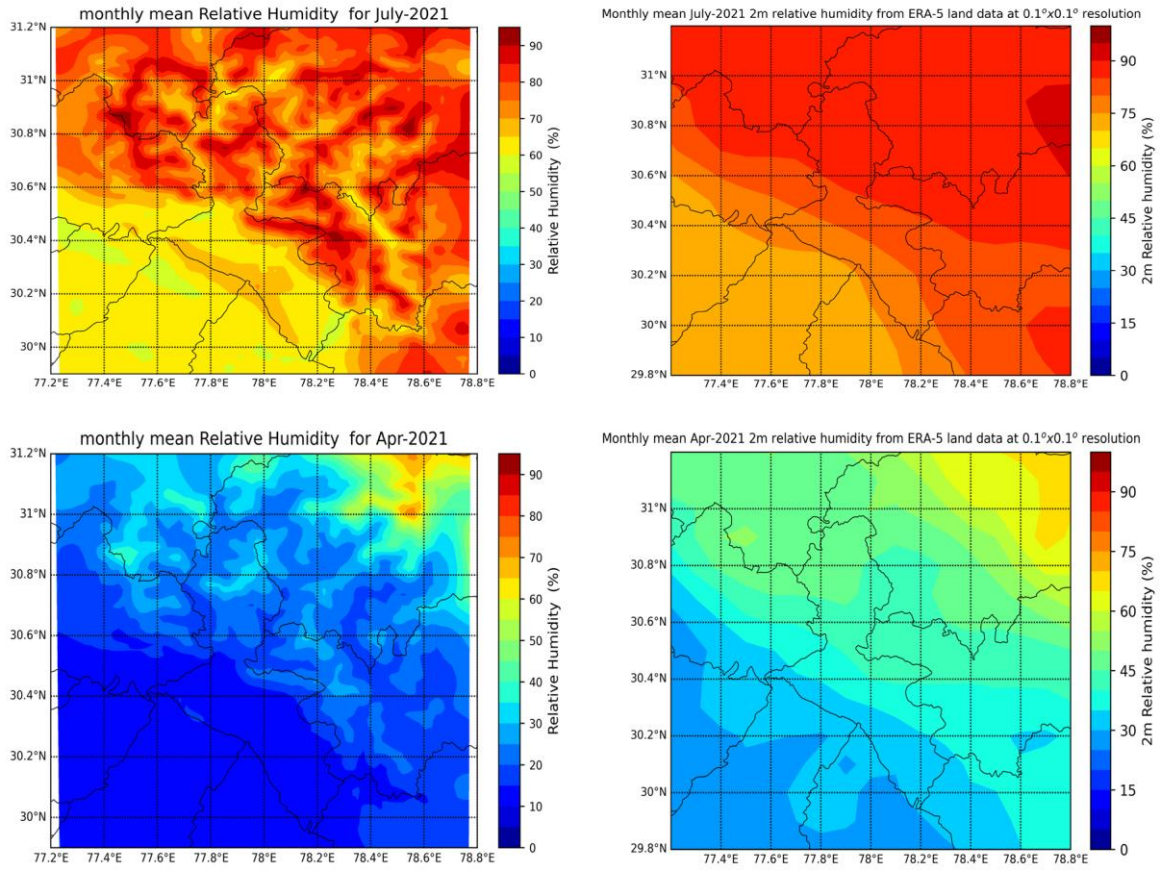

Fig. 5. Comparison of 2 m relative humidity from WRF (2×2 km² resolution) simulation (left) and ERA-5 (0.1°×0.1°) resolution (right) for July 2021 (monsoon season) (upper panels) and April 2021 (pre-monsoon season) (lower panels).

3.2. Evaluation of WRF simulation with ground observations

The year-long (1 January 2021 through 30 December 2021) validation of WRF-simulated 2 m temperature was compared with observations from two ground-based meteorological stations of the India Meteorological Department (IMD) within the simulated domain. Figure 6 presents the WRF-simulated hourly temperature variations (2 m temperature) versus the ground meteorological observations for 2021 at two locations, Dehradun Mokhampur and Mussoorie. The model was validated against ground observations for hourly temperature, the daily median temperature, and the daily peak 90th percentile temperature. The validation metrics (*r*, *IOA*, *MAE*, and *RMSE*) for both locations are presented in Table 1. The hourly temperature simulations provide insight into the model's ability to capture diurnal variations,

but daily median temperature is a robust metric better reflecting the central tendency of temperature variations while minimizing the influence of extreme values. The 90th percentile temperature represents peak daytime warming events, which are crucial for assessing extreme heat conditions.

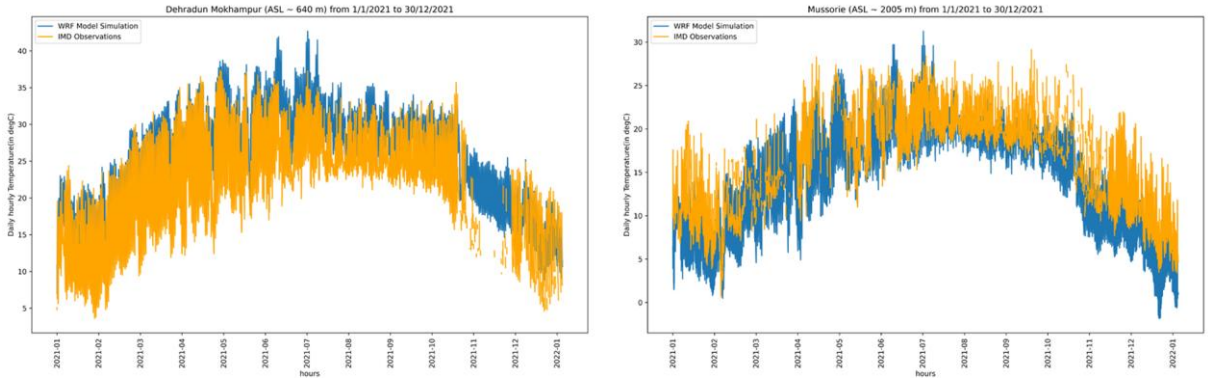

Fig. 6. The time series of hourly 2 m temperature variations obtained from WRF simulation and the observations from the IMD meteorological stations from 1 January 2021 through 30 December 2021 at Dehradun (left) and Mussoorie (right).

The comparison between WRF-simulated and observed temperatures shows that WRF performs reasonably well in both locations but exhibits greater discrepancies in Dehradun compared to Mussoorie. The correlation coefficient and *IOA* are relatively high for both locations (Table 1), indicating a general agreement between simulations and observations. The *MAE* and *RMSE* are larger for Dehradun than Mussoorie (Table 1), suggesting that WRF is less precise in urban conditions. The validation metric results for daily median temperature show that the correlation and *IOA* remain high, but slightly better than for hourly temperatures, indicating that WRF can capture the overall temperature trend more accurately. The errors (*MAE* and *RMSE*) are still higher for Dehradun, implying that urban dynamics such as heat retention and urban canyon effect are not well represented in the model. The validation metrics for daily peak 90th percentile temperature reveal lower correlation and *IOA* compared to median temperature, indicating greater difficulty in capturing peak temperature events. The error metrics were larger, especially in Dehradun, where extreme daytime temperatures are more affected by urban morphology.

For Mussoorie, WRF performs better, likely because WRF accurately incorporates the land-atmosphere interactions over complex mountainous terrain. However, for the Dehradun region, the *MAE* and *RMSE* are higher, possibly because the city has grown rapidly and the WRF simulation has not included all of the urban features. In the next section, the performance of the WRF simulation, after including urban features, is discussed.

3.3. Impact of urban features: WRF-UCM (BEP) simulation and its evaluation

The WRF-UCM with BEP scheme incorporates urban morphology by considering three-dimensional urban structures, urban canyon effects, and heat exchange between buildings and the atmosphere. The WRF-UCM with BEP scheme was run for the pre-monsoon season (22 Mar 2021 to 20 Jun 2021, where

the period 22 Mar 2021 to 31 Mar 2021 is the model's spin-up period) to assess the urban effects as effectively as possible. The impact of these modifications is assessed using key statistical metrics: *r*, *IOA*, *MAE*, and *RMSE* for three temperature categories: hourly temperature, daily median temperature, and daily peak 90th percentile temperature (Fig. 7).

Table 1. Validation metrics of WRF simulations against IMD observations for 2021.

Location	Metric	Hourly T2	Daily Median T2	Daily 90th Percentile T2
Dehradun	*r*	0.80	0.84	0.71
	IOA	0.72	0.77	0.65
	MAE (°C)	4.9	5.3	6.1
	RMSE (°C)	5.7	5.7	6.8
	MAPE (%)	14.2	12.7	15.8
	NRMSE (%)	13.5	12.9	15.1
Mussoorie	*r*	0.87	0.89	0.81
	IOA	0.79	0.83	0.74
	MAE (°C)	3.4	3.1	4.2
	RMSE (°C)	4.2	3.9	4.8
	MAPE (%)	9.8	8.9	10.7
	NRMSE (%)	10.4	9.2	11.0

Table 2. Comparison of validation metrics for WRF and WRF-UCM (BEP) during the pre-monsoon season (March-June 2021) at Dehradun and Mussoorie.

Location	Variable	Model	*r*	*IOA*	*MAE* (°C)	*RMSE* (°C)	*MAPE* (%)	*NRMSE* (%)
Dehradun	Hourly T2	WRF	0.80	0.72	4.9	5.7	14.2	13.5
		WRF-UCM (BEP)	0.83	0.78	4.1	4.9	12.0	11.6
	Median T2	WRF	0.84	0.73	5.3	5.7	13.0	13.2
		WRF-UCM (BEP)	0.86	0.78	4.3	4.7	11.4	11.0
	90th Percentile T2	WRF	0.71	0.65	6.1	6.8	15.8	15.1
		WRF-UCM (BEP)	0.78	0.70	5.0	5.9	13.2	13.0
Mussoorie	Hourly T2	WRF	0.87	0.79	3.4	4.2	9.8	10.4
		WRF-UCM (BEP)	0.88	0.80	3.2	4.0	9.4	9.9
	Median T2	WRF	0.89	0.81	3.1	3.9	9.2	9.4
		WRF-UCM (BEP)	0.90	0.82	3.0	3.8	8.8	9.1
	90th Percentile T2	WRF	0.81	0.74	4.2	4.8	10.7	11.0
		WRF-UCM (BEP)	0.82	0.75	4.0	4.6	10.3	

At Dehradun, for hourly temperature simulation, the WRF-UCM (BEP) scheme demonstrates a marginal improvement in *IOA* (0.72 to 0.78) and r (0.80 to 0.83) over the standard WRF model (Table 2). The noticeable reduction in *MAE* (4.9 to 4.1) and *RMSE* (5.7 to 4.9) for the WRF-UCM (BEP) simulation suggests a more accurate representation of diurnal temperature variations. This improvement is the result of including urban heat storage and canyon radiative trapping in the WRF through UCM (BEP scheme). At Mussoorie, the improvement is less or negligible, indicating that BEP modifications primarily benefit urban regions, where the representation of building-energy interactions is crucial. The performance

remains comparable to WRF, as the model is already capable of simulating natural terrain with limited urban influence. For daily median temperature at Dehradun, noticeable improvement is observed with WRF-UCM (BEP), as reflected in higher *IOA* values (0.53 to 0.58). The reduction in *MAE* (5.3 to 4.3) and *RMSE* (5.7 to 4.7) indicates a more precise simulation of overall daily temperature trends. The standard WRF model underestimates urban heat retention, leading to biases that BEP corrects. At Mussoorie, the results remain relatively unchanged compared to WRF, reinforcing that the urban modifications in BEP are less relevant in high-altitude, rural settings. For daily peak 90th percentile temperature performance at Dehradun, the inclusion of BEP significantly improves high-temperature peak prediction. The urban heat island (UHI) effect amplifies peak temperatures in cities, which WRF-UCM (BEP) captures better than the standard WRF model. The reduction in *MAE* and *RMSE* highlights the importance of including urban morphology in WRF for accurate extreme temperature simulation. At Mussoorie, the differences between WRF and WRF-UCM (BEP) are minor, reaffirming that urban parameterization has little influence at a hill station where urbanization is less, and therefore, the urban effect is less pronounced. The BEP scheme improves WRF's performance significantly in Dehradun by incorporating urban physics, whereas its impact in Mussoorie is minimal. Hourly and peak temperatures benefit the most from urban modifications, as they are more sensitive to urban heat storage and canyon effects.

Figure 7 illustrates the spatial distribution of the daily peak 90th percentile temperature over Dehradun averaged for May 2021, as simulated by the WRF and WRF-UCM (BEP). The results highlight the temperature variations across the region, emphasizing the impact of urbanization on local thermal conditions. The upper panels of Figure 7 compare the temperature distribution from WRF (left) and WRF-UCM (BEP scheme) (right) for the entire Dehradun region. Both simulations depict a clear spatial gradient, with elevated temperatures in the southern urban areas and cooler temperatures in the northern high-altitude regions. However, the inclusion of the urban canopy model (BEP scheme) leads to a more pronounced urban morphology effect, with higher temperatures over the city center compared to the standard WRF simulation.

The lower panel of Figure 7 focuses on the section of Dehradun that includes the urban core of Dehradun, where the temperature differences between the WRF and WRF-UCM (BEP) simulations become more apparent. The WRF-UCM simulation shows systematically higher temperatures in built-up areas due to better representation of urban geometry, thermal properties of buildings, and reduced evaporative cooling. In contrast, the standard WRF model underestimates these effects, leading to relatively lower temperatures. The enhanced warming in the WRF-UCM simulation is consistent with the urban heat island phenomenon, which is driven by increased sensible heat flux and a lower fraction of latent heat flux in urban environments.

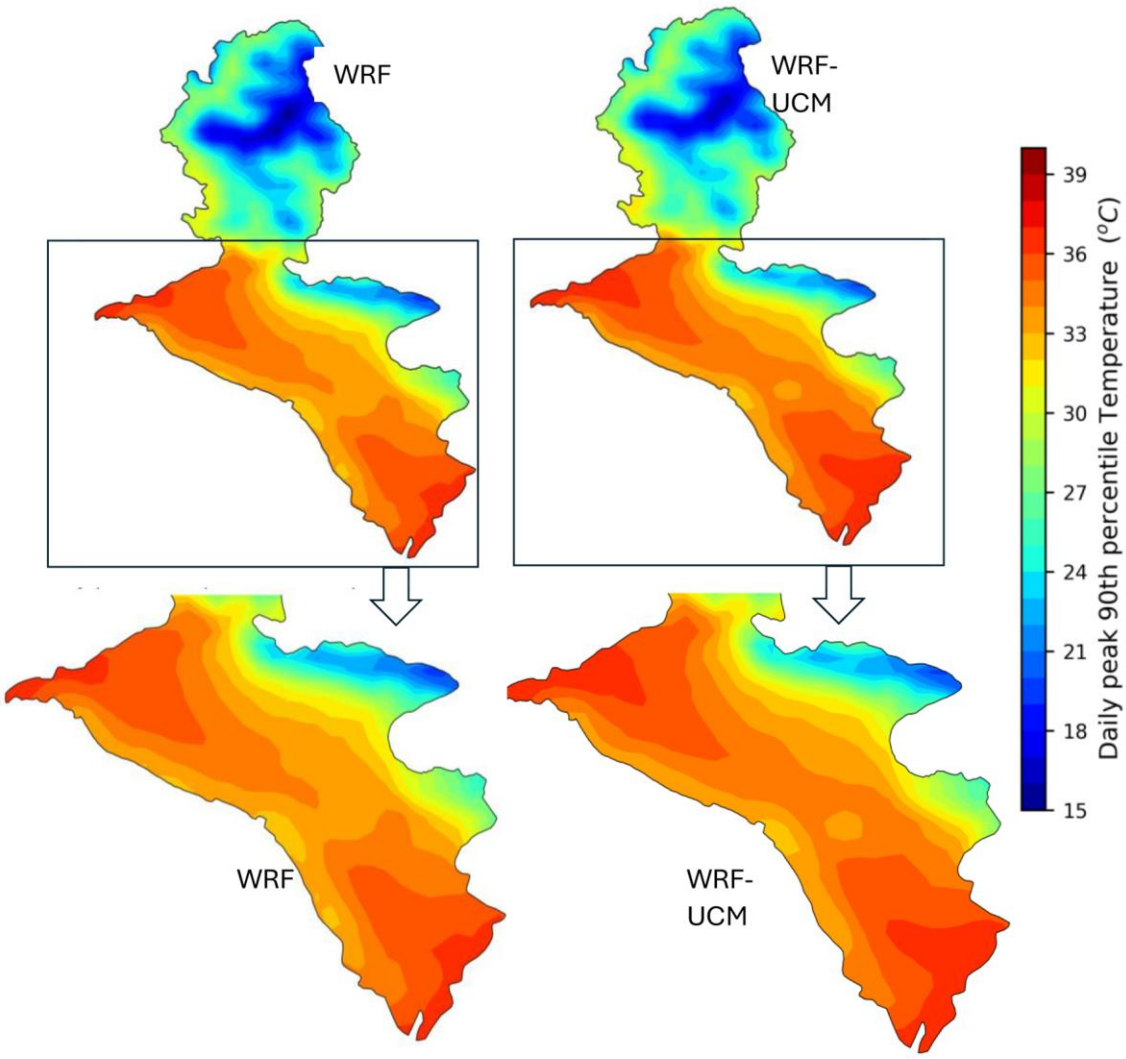

Fig. 7. May 2021 mean of daily peak 90th percentile temperature of Dehradun by WRF and WRF-UCM (BEP). The upper panel shows all of Dehradun; the lower panel shows the urban core of Dehradun that experiences higher temperatures.

3.4. Assessment of UHI effect

The UHI effect was evaluated in two complementary ways: (1) UHI based on near-surface air temperature (2-m temperature (T2)) to assess the atmospheric manifestation of the phenomenon, and (2) Surface UHI based on skin temperature (TSK) and satellite-derived MODIS LST to examine the radiative surface imprint of urban warming. Both approaches provide a comprehensive understanding of nocturnal UHI dynamics. The UHI effect is evaluated for the Dehradun city areas (municipal localities) where build-up is predominant and administratively regulated by urban municipal corporations.

3.4.1. UHI (air temperature-based):

During April, the WRF-BEP simulation produced higher nocturnal UHI intensities compared to the control WRF run, with maximum ΔT exceeding 6 K at 00:00 UTC (05:30 IST) (Fig. 8). The enhancement is attributable to the representation of urban canopy processes in BEP, which trap heat more effectively during nighttime. The UHI then diminished rapidly after sunrise, reaching near-neutral or slightly negative

values between 04:00 – 10:00 UTC (09:30 – 15:30 IST), before re-emerging in the late afternoon. Spatial maps for April indicate a clear warming core over central Dehradun, more pronounced in WRF-BEP, highlighting the importance of urban morphology in shaping near-surface temperature fields (Fig. 8).

In May, both WRF and WRF-BEP runs reproduced consistent nocturnal UHI peaks, but the magnitude was slightly lower than in April, with maximum ΔT values of about 4-4.5 K. Interestingly, the WRF simulation exhibited somewhat larger UHI magnitudes than WRF-BEP during late evening hours. This reversal suggests seasonal modulation, where stronger background heating in May reduces the relative contribution of urban canopy effects. Spatial plots show localized hot-spots over the city core during afternoon hours, although the areal extent of elevated temperatures remains broader in WRF compared to the more spatially confined but sharper warming simulated by WRF-BEP.

By June, the nocturnal UHI weakened further, with peak intensities generally below 3.5 K. The WRF control runs simulated higher UHI magnitudes than WRF-BEP, particularly during late evening (18:00 – 22:00 UTC). The weaker UHI during June can be attributed to enhanced convective activity and stronger mixing, which diminished the urban–rural thermal contrast. Spatial fields for June confirm this, showing more diffuse warming signatures with reduced intensity compared to April and May. The observational analyses in an earlier study (Dhankar et al. 2024) report that increased cloud cover and moisture during the monsoon transition dampen UHI signatures in Dehradun, matching the attenuation we diagnose in June.

Across all months, the UHI was strongest during the late evening and early nighttime hours, while it weakened substantially during the forenoon and was nearly absent around sunrise.

These results indicate a strong seasonal (monthly) modulation of UHI intensity, with maximum nocturnal intensities in April, a moderate decline in May, and a further reduction in June. The inclusion of the BEP scheme enhances the simulation of nocturnal warming during April, when stable atmospheric conditions prevail, but produces weaker signals during late pre-monsoon months when convective mixing dominates. This highlights the sensitivity of UHI representation to both urban canopy processes and background meteorological conditions. Prior Dehradun-focused UHI works (Mishra, Arya 2024) emphasize the role of built-up growth and vegetation gradients in setting the magnitude and timing of thermal contrasts; our ambient UHI diagnostics reproduce those space-time features at high resolution and attribute the April peak to stronger stability and reduced evaporative cooling over the urban core.

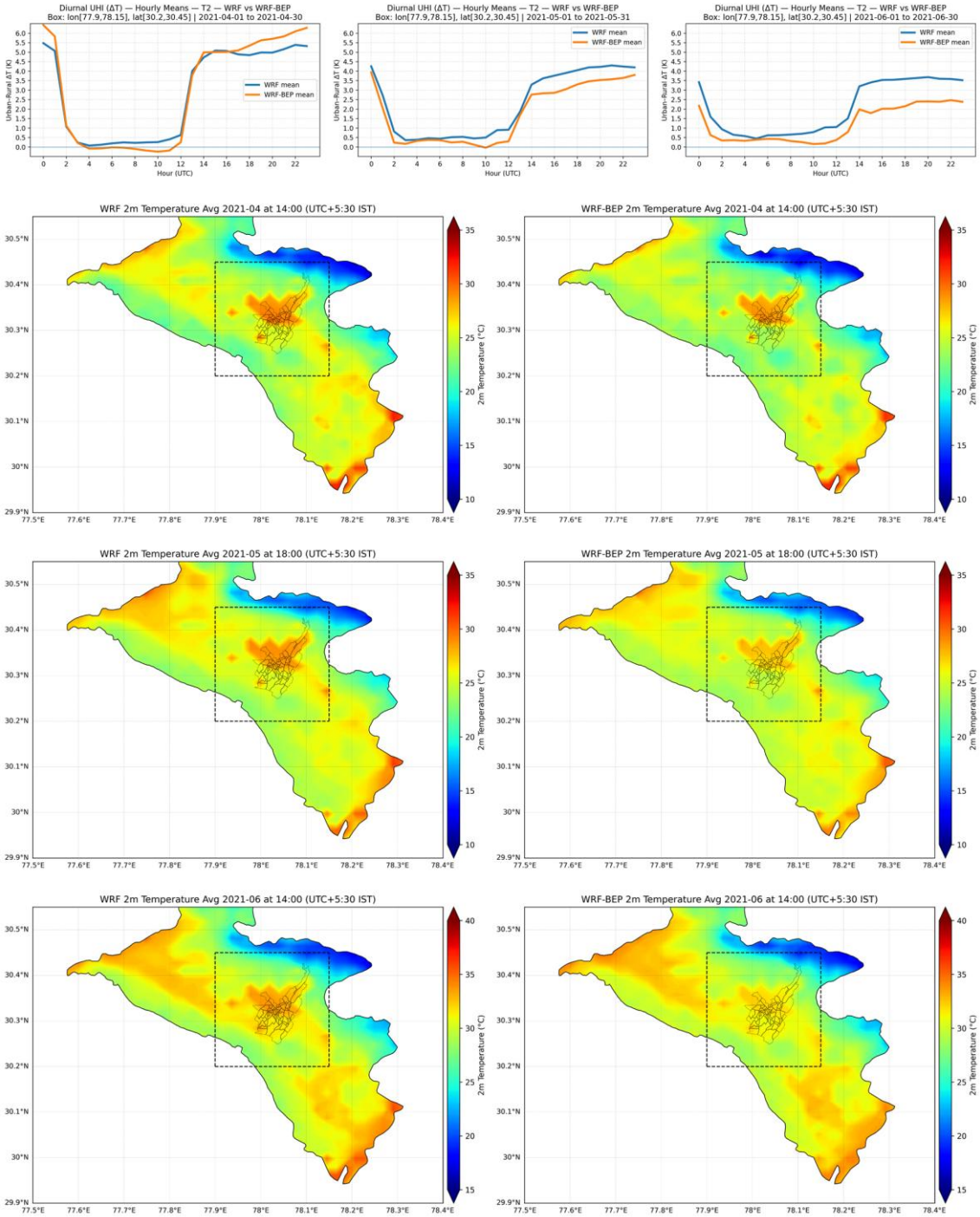

Fig. 8. Monthly variation of evening-time ambient urban heat-island (UHI) intensity ($\Delta T = T_{urban} - T_{rural}$) derived from WRF and WRF-UCM-BEP simulations for the pre-monsoon months of April, May, and June 2021. The top panel represents the monthly averaged diurnal cycles of ambient ΔT, showing stronger daytime and evening UHI development in the WRF-UCM-BEP run than in the standard WRF simulation. The lower panels include sets of maps illustrating spatial distributions of UHI intensity at 14:00 UTC (≈ 19:30 IST) for the same months, enabling consistent inter-month comparisons under peak-heating conditions. Warm anomalies exceeding 4-6°C are concentrated over the Dehradun urban core, while weaker contrasts occur in June due to enhanced convective mixing. The WRF-UCM-BEP configuration produces a more compact and realistic UHI footprint, emphasizing the role of urban morphology in regulating late-afternoon ambient temperature.

3.4.2. Surface UHI (skin temperature/MODIS LST)

To assess the surface expression of the UHI, we compared monthly composites of MODIS 1-km LST with modeled skin temperature (TSK) from the control WRF run and the urban-canopy run (WRF-BEP) over Doon Valley.

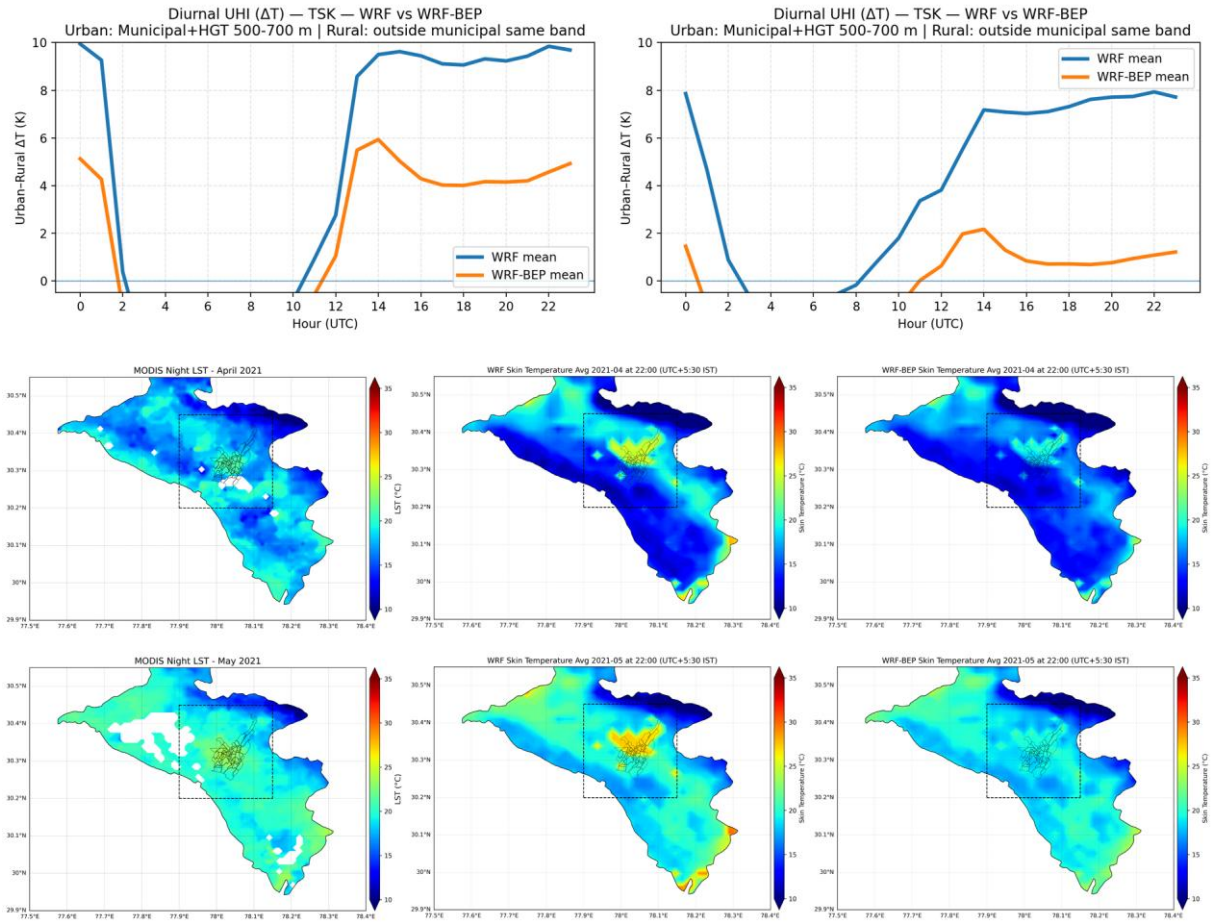

Fig. 9. Monthly variation of nighttime surface UHI ($\Delta T\_skin = TSK_{urban} - TSK_{rural}$) from WRF and WRF-UCM-BEP simulations compared with MODIS 1 km land-surface-temperature (LST) for April and May 2021. The top panel shows the monthly average diurnal cycles of surface ΔT_skin, demonstrating stronger nocturnal UHI intensity and slower post-sunset cooling in the WRF-UCM-BEP simulation. The subsequent maps depict spatial distributions of nighttime surface UHI at 01:00 UTC (≈ 06:30 IST) for each month. MODIS LST (Aqua night 1:30 to 1:50 local overpass time) maps (top row of each month) serve as observational references; WRF and WRF-UCM-BEP maps illustrate modeled skin-temperature and UHI intensity fields. The WRF-UCM-BEP configuration captures a compact, warmer surface core centered over Dehradun in close agreement with MODIS observations, whereas the control WRF run exhibits diffuse heating extending into rural surroundings. These results confirm the improved capability of the BEP scheme to reproduce nocturnal surface-UHI magnitude, structure, and monthly variability under pre-monsoon conditions.

The surface UHI was computed as $\Delta T_{surf} = \bar{T}_{urban} - \bar{T}_{rural}$. We focus on April and May 2021, when the pre-monsoon dry and clear conditions make surface temperature contrasts most distinct.

Hourly means of surface ΔT (urban − rural) from modeled skin temperature show a clear pre-monsoon diurnal rhythm. In April, ΔT builds from late morning, peaks during late afternoon and early evening, and then weakens overnight; May follows the same shape with a slightly muted amplitude, while June is flatter and weaker as humidity and cloudiness rise toward the monsoon. Over these months, the control WRF generally produces a larger and more persistent afternoon plateau than expected. Adding the urban canopy (WRF-BEP) dampens the peak by roughly 20-40% in April and May and slightly sharpens the rise and decay, yielding timing and magnitude that align better with typical dry-season surface heating over the valley. A 2020 Dehradun analysis (Maithani et al. 2020) using Landsat/MODIS shows compact, recurrent hot-spots over the municipal corridor with the strongest pre-monsoon contrasts and a damped diurnal amplitude as humidity increases – patterns mirrored by our MODIS-constrained evaluation and improved by WRF-BEP.

The spatial LST fields for April and May reinforce this behavior. MODIS 1-km (Aqua night: 1:30 to 1:50 local overpass time) composites consistently show a compact warm core along the Dehradun urban corridor, with cooler forested slopes and higher terrain surrounding it. The control WRF reproduces a warm center but spreads it too broadly and sometimes displaces warmth onto adjacent hills, indicating an overly diffuse hot-spot and mild warm bias outside built-up areas. WRF-BEP concentrates the hot-spot more tightly over the valley floor, reduces spurious warming on the slopes, and matches the observed placement of the warm core more closely in both months.

Thus, WRF-BEP explains the surface UHI more credibly than the control WRF: it lowers exaggerated afternoon ΔT, improves the timing of the diurnal cycle, and better captures the compact spatial footprint of the urban warm core observed by MODIS, while limiting artificial spillover of heating onto surrounding terrain. A recent Dehradun-specific study (Singh et al. 2024a) documents seasonal dynamics and multi-decadal warming of surface thermal conditions, with intensified warm cores coincident with expansion of built-up areas in the valley floor; our MODIS, WRF-BEP comparison reproduces those compact hot-spots and their pre-monsoon amplification, indicating that explicit urban morphology helps constrain both magnitude and footprint of surface UHI in Dehradun.

3.5. Role of mountain-breeze circulation and the dominance of urban morphology in regulating valley temperature

The Doon Valley's north-south relief, bounded by the Siwalik Hills and Mussoorie Range, supports strong diurnal thermally driven winds, i.e., daytime upslope (anabatic) and nighttime downslope (katabatic) flows, that naturally ventilate the basin (Karki et al. 2017; Singh et al. 2021). Under clear pre-monsoon conditions, these circulations promote nocturnal cooling and maintain valley-slope temperature contrasts.

In the standard WRF simulation, the nocturnal pattern at 01:00 UTC on 15 May 2021 (Fig. 10a) clearly depicts cooler air pooled within the valley and a temperature gradient toward the northern slopes, indicating organized katabatic drainage. The WRF-UCM (BEP) run (Fig. 10b) alters this structure substantially: valley temperatures remain elevated, horizontal gradients flatten, and the difference map

(Fig. 10c) reveals localized warming of +1.5-2°C across the urbanized Doon-Rispana corridor. Cooler anomalies confined to forested ridges imply that radiative trapping and heat storage within built surfaces suppress nocturnal cold-air formation.

Vertical cross-sections of temperature and potential temperature (Fig. 11) reinforce these contrasts. The control WRF simulation shows a shallow inversion around 700-800 m ASL and steep potential-temperature gradients typical of stable stratification. In WRF-BEP, this inversion nearly vanishes, and vertical gradients weaken, producing a more mixed boundary layer. The added urban heat flux erodes surface stability and limits nocturnal cooling.

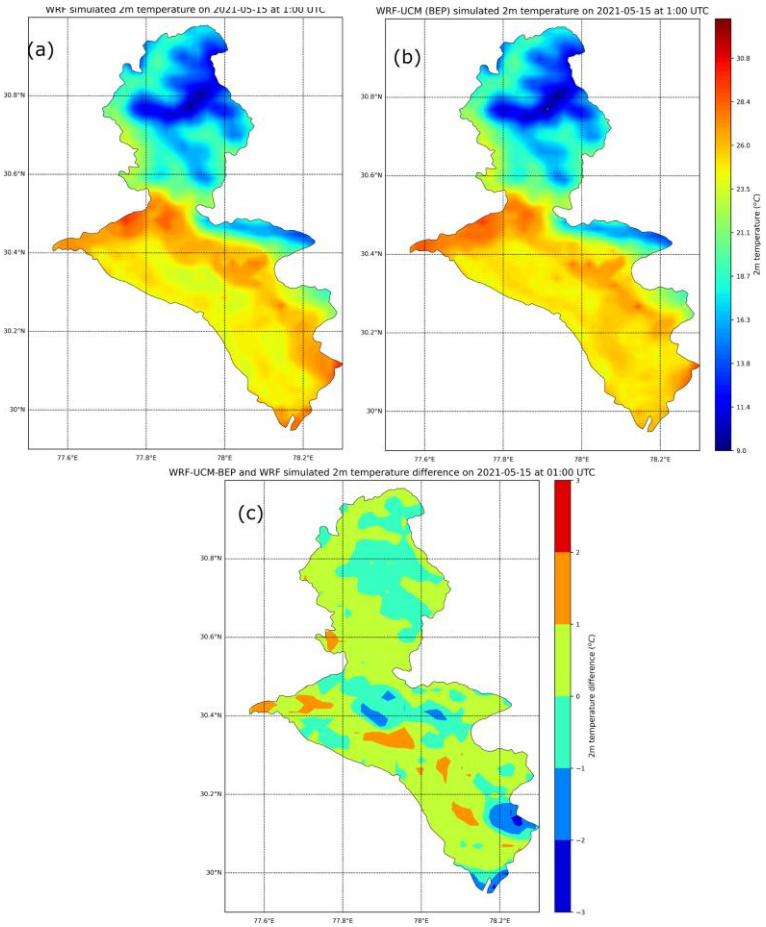

Fig. 10. Simulated 2 m temperature (WRF) at 01:00 UTC on 15 May (a); Simulated 2 m temperature (WRF-BEP) at 01:00 UTC on 15 May 2025 (b); Difference in 2 m temperature (WRF-BEP − WRF) (c).

The wind cross-sections (Fig. 12) depict a similar transition. In WRF, downslope winds of ~1-2 m s^{-1} descend from the Mussoorie slopes toward the valley floor, forming a coherent mountain-breeze cell. In WRF-BEP, these flows become disorganized and weaker, occasionally reversing near the surface above the city core. Difference plots (Figs. 13-14) quantify this effect: warming of +1-2°C and wind-speed reductions up to 1.8 m s^{-1} within 0-2 km AGL show that urban heat alters both thermal and dynamical structures. Surface warming enhances near-surface stability, weakening katabatic momentum and reducing natural nighttime ventilation.

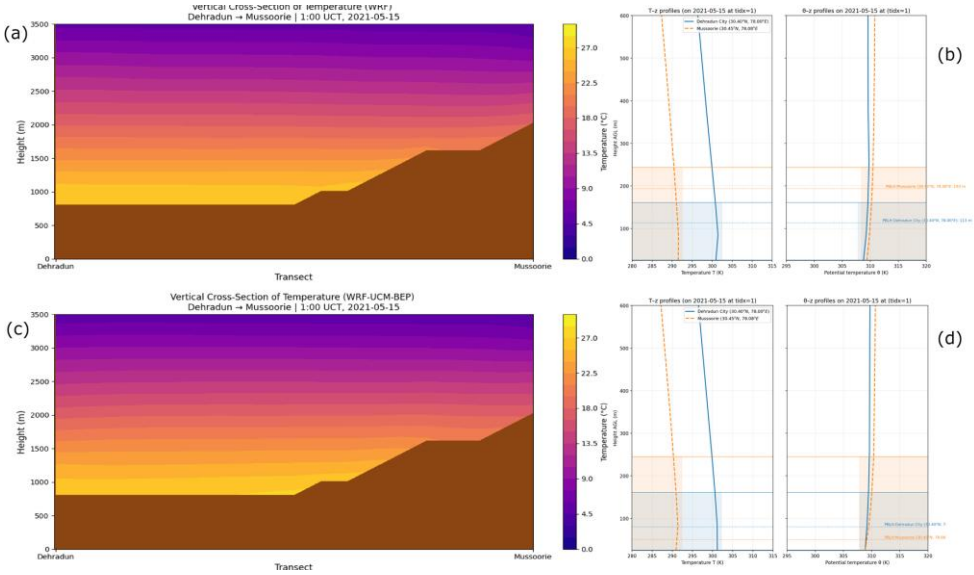

Fig. 11. (a) Vertical cross-section of temperature (from WRF run); (b) temperature vs. height (from surface) and θ (potential temperature) vs. height (from surface) profile (from WRF run); (c) vertical cross-section of temperature (from WRF-UCM-BEP run); (d) temperature vs. height (from surface) and θ (potential temperature) vs. height profile (from surface) (from WRF-UCM-BEP). The temperature inversion is suppressed in the WRF-UCM-BEP run.

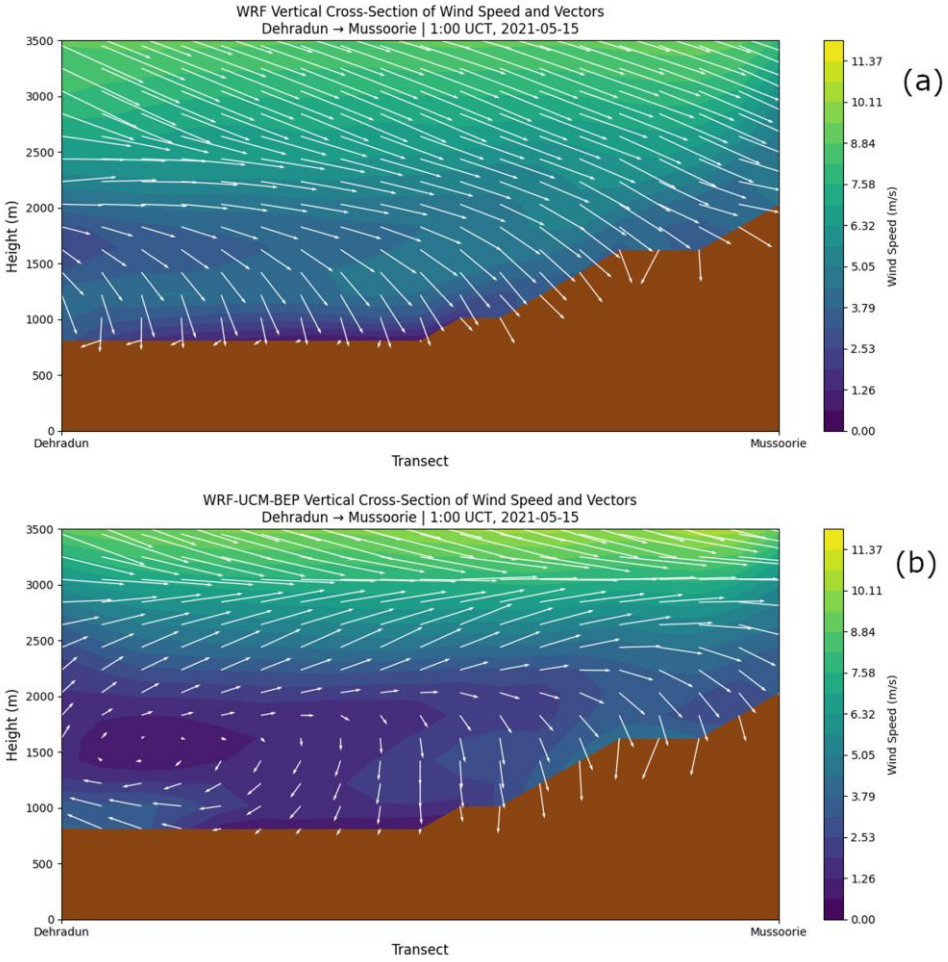

Fig. 12. (a) Vertical cross-section of wind speed and vectors (WRF), (b) Vertical cross-section of wind speed and vectors (WRF-BEP).

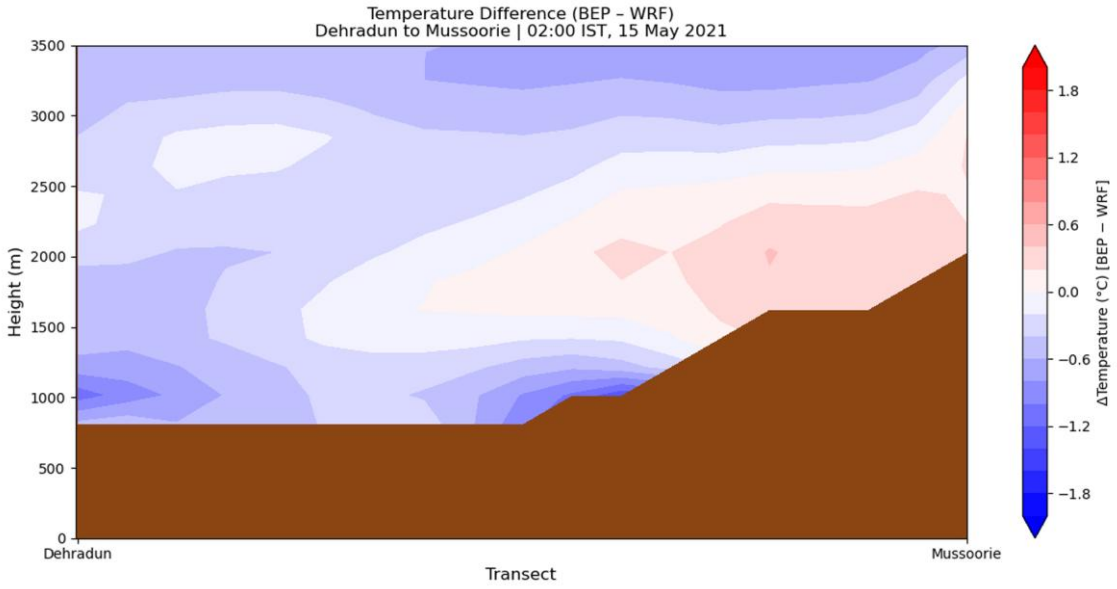

Fig. 13. Vertical cross-section of temperature difference (WRF-BEP − WRF).

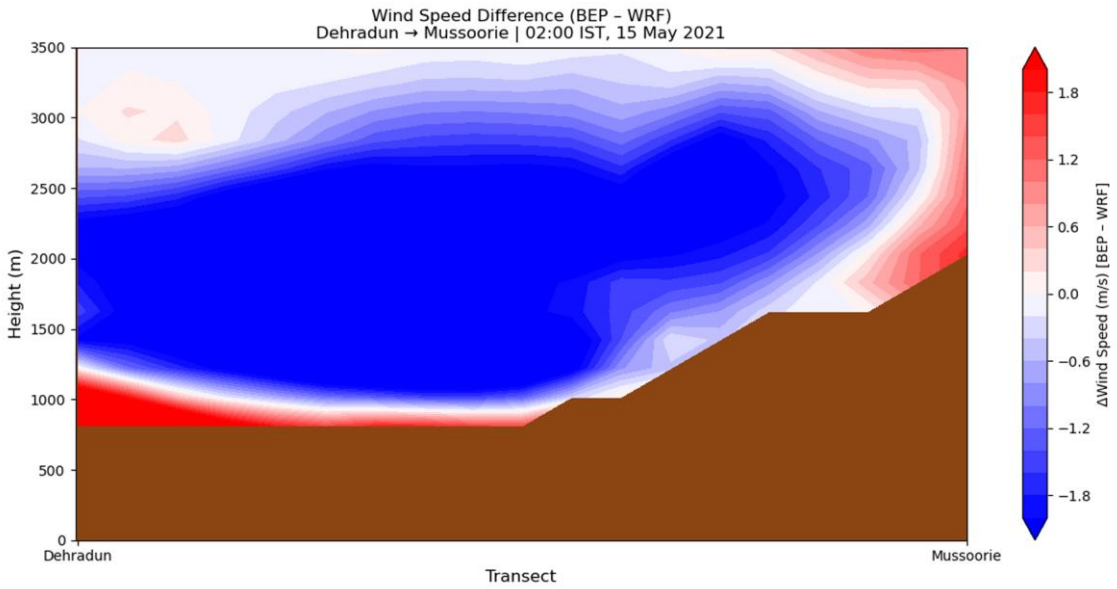

Fig. 14. Vertical cross-section of wind speed difference (WRF-BEP − WRF).

Collectively, these diagnostics demonstrate that urban morphology dominates over terrain-induced thermodynamics in controlling nocturnal conditions within the Doon Valley. The multilayer BEP scheme captures how building geometry, high heat capacity, and canyon radiation trapping disrupt cold-air drainage and maintain persistent nighttime warmth. Such suppression of mountain-breeze circulation implies reduced ventilation efficiency, elevated heat stress, and potential deterioration of nighttime air quality.

Comparable results have been reported for other mountainous cities – Lisbon (Silva et al. 2021), Manila (Bilang et al. 2022), and Athens (Roukounakis et al. 2023) – but this study extends the evidence to the western Himalayas, demonstrating how rapid urbanization can override natural cooling processes in

intermontane basins. The findings highlight the necessity of incorporating realistic urban morphology in mesoscale modeling to accurately represent thermal dynamics and inform climate-responsive urban planning for Himalayan valleys such as Dehradun.

The analysis revealed that the WRF-BEP framework provides a more realistic representation of urban–topography interactions in the Doon Valley, highlighting the dominance of built environment characteristics in controlling nocturnal temperature and wind patterns. These findings have critical implications for urban planning, nighttime heat stress management, and air quality regulation, particularly in rapidly urbanizing intermontane basins like Dehradun.

4. Conclusion

This study demonstrates the capability of high-resolution (2×2 km^2) WRF model simulations, configured with a threefold nested domain (18-6-2 km) and NCEP-FNL (0.25°) boundary conditions, to capture the complex meteorological and thermal dynamics of the Doon Valley, a rapidly urbanizing intermontane basin in the western Himalayas. The model effectively resolved the valley's topographic gradients and diurnal variability, providing a robust basis to assess how urban morphology modifies local temperature regimes.

The integration of the Urban Canopy Model coupled with the Building Effect Parameterization (WRF-UCM-BEP) substantially enhanced model fidelity, particularly in Dehradun (urbanized valley). Quantitative validation against India Meteorological Department (IMD) observations showed improvements in correlation ($r = 0.83 \rightarrow 0.86$) and index of agreement ($IOA = 0.72 \rightarrow 0.78$), along with a 15-20% reduction in MAE and $RMSE$ for ambient (2 m) air temperature. These improvements were most pronounced during the pre-monsoon season, when urban heat storage, radiative trapping, and reduced evaporative cooling strongly influence temperature extremes. In contrast, the Mussoorie (hill station) site exhibited negligible improvement, underscoring that WRF-UCM-BEP primarily benefits simulations in urbanized low-lying valleys where built morphology governs local energy exchange.

The WRF-UCM-BEP configuration successfully reproduced the ambient urban heat island (UHI) in Dehradun, characterized by persistent nocturnal warming of 1-2°C and improved simulation of diurnal temperature cycles. It also improved the surface UHI representation by producing a compact and spatially coherent warm core that closely aligned with MODIS 1-km land surface temperature (LST) observations. This dual agreement between ambient and surface temperature patterns confirms the model's effectiveness in capturing both the atmospheric and radiative imprints of urbanization.

Vertical diagnostics further revealed that WRF-UCM-BEP improved the representation of boundary-layer structure, capturing realistic vertical mixing profiles while weakening katabatic winds (-1.5 to -2 m s^{-1}) and suppressing nocturnal inversion layers that ordinarily develop under stable nighttime conditions. The resulting disruption of mountain-breeze circulation indicates that urban morphology reduces nocturnal cooling and natural ventilation, thereby intensifying heat retention within the valley atmosphere.

Collectively, these findings highlight that urban morphology exerts a dominant control on both ambient and surface thermal environments in Dehradun, while exerting minimal influence over higher, less-urbanized terrain such as Mussoorie. The results emphasize the necessity of incorporating multilayer urban canopy schemes into high-resolution mesoscale models for topographically complex and rapidly urbanizing regions.

In addition to improving model realism, these insights have direct implications for urban planning, heat-stress mitigation, and air-quality management in Himalayan cities. Integrating urban morphological parameters into weather and climate modeling frameworks can support climate-resilient design strategies, improve urban ventilation planning, and inform sustainable growth policies for intermontane basins such as the Doon Valley.

References

Arthur R.S., Lundquist K.A., Mirocha J.D., Chow F.K., 2018, Topographic effects on radiation in the WRF model with the immersed boundary method: implementation, validation, and application to complex terrain, Monthly Weather Review, 156, 3277-3292, DOI: 10.1175/MWR-D-18-0108.1.

Bilang R.G.J.P., Blanco A.C., Santos J.A.S., Olaguera L.M.P., 2022, Simulation of Urban Heat Island during a high-heat event using WRF urban canopy models: a case study for Metro Manila, Atmosphere, 13 (10), DOI: 10.3390/atmos13101658.

Biswasharma R., Umakanth N., Pongener I., Longkumer I., Rao K.M.M., Pawar S.D., Gopalkrishnan V., Sharma S., 2024, Sensitivity analysis of cumulus and microphysics schemes in the WRF model in simulating Extreme Rainfall Events over the hilly terrain of Nagaland, Atmospheric Research, 304, DOI: 10.1016/j.atmosres.2024.107393.

Borrego C., Monteiro A., Ferreira J., Miranda A.I., Costa A.M., Carvalho A.C., Lopes M., 2008, Procedures for estimation of modelling uncertainty in air quality assessment, Environment International, 34 (5), 613-620, DOI: 10.1016/j.envint.2007.12.005.

Brown C.F., Brumby S.P., Guzder-Williams B., Birch T., Hyde S.B., Mazzariello J., Czerwinski W., Pasquarella V.J., Haertel R., Ilyushchenko S., Schwehr K., Weisse M., Stolle F., Hanson G., Guinan O., Moore R., Tait A.M., 2022, Dynamic World, near real-time global 10 m land use land cover mapping, Scientific Data, 9, DOI: 10.1038/s41597-022-01307-4.

Dhankar S., Singh G., Kumar K., 2024, Impacts of urbanization on land use, air quality, and temperature dynamics in Dehradun district of Uttarakhand, India: a comprehensive analysis, Frontiers in Environmental Science, 12, DOI: 10.3389/fenvs.2024.1324186

Dilawar A., Chen B., Guo L., Liu S., Shafeeque M., Arshad A., Hussain Y., Qureshi M.A., Kayiranga A., Wang F., Measho S., Zhang H., 2021, Evaluation the WRF model with different land surface schemes: Heat wave event simulations and its relation to pacific variability over Ccoastal region, Karachi, Pakistan, Sustainability, 13 (22), DOI: 10.3390/su132212608.

Ek M.B., Mitchell K.E., Lin Y., Rogers E., Grunmann P., Koren V., Gayno G., Tarpley J.D., 2003, Implementation of Noah land surface model advances in the National Centers for Environmental Prediction operational mesoscale Eta model, Journal of Geophysical Research: Atmospheres, 108 (D22), DOI: 10.1029/2002JD003296.

Farr T.G., Rosen P.A., Caro E., Crippen R., Duren R., Hensley S., Kobrick M., Paller M., Rodriguez E., Roth L., Seal D., Shaffer S., Shimada J., Umland J., Werner M., Oskin M., Burbank D., Alsdorf D.E., 2007, The shuttle radar topography mission, Reviews of Geophysics, 45 (2), DOI: 10.1029/2005RG000183.

Garuma G.F., 2018, Review of urban surface parameterizations for numerical climate models, Urban Climate, 24, 830-851, DOI: 10.1016/j.uclim.2017.10.006.

Gaur A., Lacasse M., Armstrong M., Lu H., Shu C., Fields A., Palou F.S., Zhang Y., 2021, Effects of using different urban parametrization schemes and land-cover datasets on the accuracy of WRF model over the City of Ottawa, Urban Climate, 35, DOI: 10.1016/j.uclim.2020.100737.

Golzio A., Ferrarese S., Cassardo C., Diolaiuti G.A., Pelfini M., 2021, Land-use improvements in the weather research and forecasting model over complex mountainous terrain and comparison of different grid sizes, Boundary-Layer Meteorology, 180, 319-351, DOI: 10.1007/s10546-021-00617-1.

Gupta P., Verma S., Mukhopadhyay P., Bhatla R., Payra S., 2024, Fidelity of WRF model in simulating heat wave events over India, Scientific Reports, 14 (1), DOI: 10.1038/s41598-024-52541-2.

Hendricks E.A., Knievel J.C., 2022, Evaluation of urban canopy models against near-surface measurements in Houston during a strong frontal passage, Atmosphere, 13 (10), DOI: 10.3390/atmos13101548.

Hong S.-Y., Dudhia J., Chen S.-H., 2004, A revised approach to ice microphysical processes for the bulk parameterization of clouds and precipitation, Monthly Weather Review, 132 (1), 103-120, DOI: 10.1175/1520-0493(2004)132<0103:ARATIM>2.0.CO;2.

Hong S.-Y., Noh Y., Dudhia J., 2006, A new vertical diffusion package with an explicit treatment of entrainment processes, Monthly Weather Review, 134 (9), 2318-2341, DOI: 10.1175/MWR3199.1.

Kain J.S., 2004 The Kain-Fritsch convective parameterization: an update, Journal of Applied Meteorology, 43 (1), 170-181, DOI: 10.1175/1520-0450(2004)043<0170:TKCPAU>2.0.CO;2.

Karki R., Hasson S., Gerlitz L., Schickhoff U., Scholten T, Böhner J., 2017, Quantifying the added value of convection-permitting climate simulations in complex terrain: a systematic evaluation of WRF over the Himalayas, Earth System Dynamics, 8 (3), 507-528, DOI: 10.5194/esd-8-507-2017.

Karppinen A., Kukkonen J., Elolähde T., Konttinen M., Koskentalo T., Rantakransa E., 2000, A modelling system for predicting urban air pollution: Model description and applications in the Helsinki metropolitan area, Atmospheric Environment, 34 (22), 3735-3743, DOI: 10.1016/S1352-2310(00)00074-1.

Lin C.-Y., Su C.-J., Kusaka H., Akimoto Y., Sheng Y.-F., Huang J.-C., Hsu H.-H., 2016, Impact of an improved WRF urban canopy model on diurnal air temperature simulation over northern Taiwan, Atmospheric Chemistry and Physics, 16 (3), 1809-1822, DOI: 10.5194/acp-16-1809-2016.

Liu H., Shang L., Li M., Zheng X., Shi P., 2024, WRF numerical simulation of summer precipitation and its application over the mountainous southern Tibetan Plateau based on different cumulus parameterization schemes, Atmospheric Research, 309, DOI: 10.1016/J.ATMOSRES.2024.107608.

Liu H., Zhao X., Duan K., Shang W., Li M., Shi P., 2023, Optimizing simulation of summer precipitation by weather research and forecasting model over the mountainous southern Tibetan Plateau, Atmospheric Research, 281, , DOI: 10.1016/J.ATMOSRES.2022.106484.

Liu S., 2024, Sensitivity of WRF-simulated 2 m temperature and precipitation to physics options over the Loess Plateau, Advances in Meteorology, 2024 (1), DOI: 10.1155/2024/6633255.

Luna M.A.G., Casallas A., Cerón L.C.B., Clappier A., 2020, Implementation and evaluation of WRF simulation over a city with complex terrain using Alos-Palsar 0.4 s topography, Environmental Science and Pollution Research, 27, 37818-37838, DOI: 10.1007/s11356-020-09824-8.

Maithani S., Nautiyal G., Sharma A., 2020, Investigating the effect of lockdown during COVID-19 on land surface temperature: study of Dehradun City, India, Journal of the Indian Society of Remote Sensing, 48 (9), 1297-1311, DOI: 10.1007/s12524-020-01157-w.

Martilli A., Clappier A., Rotach M.W., 2002, An urban surface exchange parameterization for mesoscale models, Boundary-Layer Meteorology, 104 (2), 261-304, DOI: 10.1023/A:1016099921195.

Min Y., Huang W., Ma M., Zhang Y., 2021, Simulations in the topography effects of Tianshan mountains on an extreme precipitation event in the Ili River valley, China, Atmosphere, 12 (6), DOI: 10.3390/atmos12060750.

Mishra A., Arya D.S., 2024, Assessment of land-use land-cover dynamics and urban heat island effect of Dehradun city, North India: a remote sensing approach, Environment, Development and Sustainability, 26 (9), 22421-22447, DOI: 10.1007/s10668-023-03558-6.

Mlawer E.J., Taubman S.J., Brown P.D., Iacono M.J., Clough S.A., 1997, Radiative transfer for inhomogeneous atmosphere: RRTM, a validated correlated-k model for the longwave, Journal of Geophysical Research: Atmospheres, 102 (D14), 16663-16682, DOI: 10.1029/97JD00237.

Monin A.S., Obukhov A.M., 1954, Basic laws of turbulent mixing in the surface layer of the atmosphere, Contributions of the Geophysical Institute, Academy of Sciences USSR, 24 (151), 163-187.

Mussetti G., Brunner D., Henne S., Allegrini J., Scott Krayenhoff E., Schubert S., Feigenwinter C., Vogt R., Wicki A., Carmeliet J., 2020, COSMO-BEP-Tree v1.0: a coupled urban climate model with explicit representation of street trees, Geoscientific Model Development, 13 (3), 1685-1710, DOI: 10.5194/gmd-13-1685-2020.

Namdev P., Sharan M., Srivastava A., Mishra S.K., 2024, An updated parameterization of the unstable atmospheric surface layer in the WRF model, Geoscientific Model Development, 17 (22), 8093-8115, DOI: 10.5194/gmd-17-8093-2024.

Navale A., Singh C., 2020, Topographic sensitivity of WRF-simulated rainfall patterns over the North West Himalayan region, Atmospheric Research, 242, DOI: 10.1016/j.atmosres.2020.105003.

NCAR, 2008, WRF Domain Wizard User Guide, National Center for Atmospheric Research, available online at https://www2.mmm.ucar.edu/wrf/users/ (data access 19.12.2025).

NCAR, 2024, available online at https://www.mmm.ucar.edu/models/wrf (data access 19.12.2025).

Noble E., Druyan L.M., Fulakeza M., 2014, The sensitivity of WRF daily summertime simulations over West Africa to alternative parameterizations. Part I: African wave circulation, Monthly Weather Review, 142 (4), 1588-1608, DOI: 10.1175/MWR-D-13-00194.1.

Ntoumos A., Hadjinicolaou P., Zittis G., Constantinidou K., Tzyrkalli A., Lelieveld J., 2023, Evaluation of WRF model boundary layer schemes in simulating temperature and heat extremes over the Middle East-North Africa (MENA) region, Journal of Applied Meteorology and Climatology, 62 (9), 1315-1332, DOI: 10.1175/JAMC-D-22-0108.1.

Politi N., Sfetsos A., Vlachogiannis D., Nastos P.T., Karozis S., 2020, A sensitivity study of high-resolution climate simulations for Greece, Climate, 8 (3), DOI: 10.3390/cli8030044.

Roukounakis N., Varotsos K.V., Katsanos D., Lemesios I., Giannakopoulos C., Retalis A., 2023, High resolution WRF modelling of extreme heat events and mapping of the Urban Heat Island characteristics in Athens, Greece, Sustainability, 15 (23), DOI: 10.3390/su152316509.

Silva R., Carvalho A.C., Carvalho D., Rocha A., 2021, Study of urban heat islands using different urban canopy models and identification methods, Atmosphere, 12 (4), DOI: 10.3390/atmos12040521.

Singh G., Ojha P.K., Sharma S.K., Kumari P., Pandey A.K., Mishra A.K., Kumar K., 2024a, Implications of urbanization on the seasonal dynamics and long-term trends in the thermal climate of a city in the Himalayan foothills of India, Journal of Geovisualization and Spatial Analysis, 8 (2), DOI: 10.1007/s41651-024-00178-0.

Singh J., Singh N., Ojha N., Dimri A.P., Singh R.S., 2024b, Impacts of different boundary layer parameterization schemes on simulation of meteorology over Himalaya, Atmospheric Research, 298, DOI: 10.1016/j.atmosres.2023.107154.

Singh J., Singh N., Ojha N., Sharma A., Pozzer A., Kiran Kumar N., Rajeev K., Gunthe S.S., Kotamarthi V.R., 2021, Effects of spatial resolution on WRF v3.8.1 simulated meteorology over the central Himalaya, Geoscience Model Development, 14 (3), 1427-1443, DOI: 10.5194/gmd-14-1427-2021.

Skamarock W.C., Klemp J.B., Dudhia J., Gill D.O., Liu Z., Berner J., Wang W., Powers J.G., Duda M.G., Barber D.M., Huang X.-Y., 2019, A description of the advanced research WRF Version 4, NCAR TECHNICAL NOTE, NCAR/TN–556+STR.

Thakur V.C., Rawat B.S., 1992, Geological Map of the Western Himalaya. Wadia Institute of Himalayan Geology, Dehradun.

Valdiya K.S., 1980, Geology of the Kumaun Lesser Himalaya, Wadia Institute of Himalayan Geology, Dehradun, India. 21 pp.

Wang Y., Brasseur G.P., Ma Y.-F., Peuch V.-H., Wang T., 2023, Does downscaling improve the performance of urban ozone modeling?, Geophysical Research Letters, 50 (23), DOI: 10.1029/2023GL104761.

Willmott C.J., 1981, On the validation of models, Physical Geography, 2 (2), 184-194, DOI: 10.1080/02723646.1981.10642213.

Zhang G., Zhu S., Zhang N., Zhang G., Xu Y., 2022, Downscaling hourly air temperature of WRF simulations over complex topography: a case study of Chongli District in Hebei Province, China, Journal of Geophysical Research: Atmospheres, 127 (3), DOI: 10.1029/2021JD035542.

Zhang X., Anagnostou E.N., Frediani M., Solomos S., Kallos G., 2013, Using NWP simulations in satellite rainfall estimation of heavy precipitation events over mountainous areas, Journal of Hydrometeorology, 14 (6), 1844-1858, DOI: 10.1175/JHM-D-12-0174.1.

Zittis G., Hadjinicolaou P., Lelieveld J., 2014, Comparison of WRF model physics parameterizations over the MENA-CORDEX domain, American Journal of Climate Change, 3 (5), 490-511, DOI: 10.4236/ajcc.2014.35042.